HHS Public Access

Author manuscript

IEEE Trans Biomed Eng. Author manuscript; available in PMC 2020 December 01.

Published in final edited form as:

IEEE Trans Biomed Eng. 2019 December ; 66(12): 3436–3443. doi:10.1109/TBME.2019.2905763.

Cardiac Tissue Chips (CTCs) for Modelling Cardiovascular Disease

Aaron J. Rogers[a,b], **Jessica M. Miller**[b], **Ramaswamy Kannappan**[b], **Palaniappan Sethu**[a,b]

[a.]Division of Cardiovascular Disease, Department of Medicine, University of Alabama at Birmingham, Birmingham, AL

[b.]Department of Biomedical Engineering, School of Engineering, University of Alabama at Birmingham, Birmingham, AL

Abstract

Objective—Cardiovascular research and regenerative strategies have been significantly limited by the lack of relevant cell culture models that can recreate complex hemodynamic stresses associated with pressure-volume changes in the heart.

Methods—To address this issue, we designed a Biomimetic Cardiac Tissue Chip (CTC) Model where encapsulated cardiac cells can be cultured in 3D fibres and subjected to hemodynamic loading to mimic pressure-volume changes seen in the left ventricle. These 3D fibres are suspended within a microfluidic chamber between two posts and integrated within a flow loop. Various parameters associated with heart function like heart rate, peak-systolic pressure, end-diastolic pressure and volume, end-systolic pressure and volume, and duration ratio between systolic and diastolic can all be precisely manipulated allowing culture of cardiac cells under developmental, normal, and disease states.

Results—We describe two examples of how the CTC can significantly impact cardiovascular research by reproducing the pathophysiological mechanical stresses associated with pressure overload and volume overload. Our results using H9c2 cells, a cardiomyogenic cell line, clearly show that culture within the CTC under pathological hemodynamic loads accurately induces morphological and gene expression changes similar to that seen in both hypertrophic and dilated cardiomyopathy. Under pressure overload the cells within the CTC see increased hypertrophic remodelling and fibrosis whereas cells subject to prolonged volume overload experience significant changes to cellular aspect ratio through thinning and elongation of the engineered tissue.

Conclusions—These results demonstrate that the CTC can be used to create highly relevant models where hemodynamic loading and unloading are accurately reproduced for cardiovascular disease modelling.

Keywords

engineered cardiac tissue; cardiac disease models; cardiomyopathy; tissue chips

Corresponding Author: Palaniappan Sethu, 1918 University Blvd, MCLM 290A, Division of Cardiovascular Disease, University of Alabama-Birmingham, Birmingham, AL 35294-0006, Ph: (205) 975-4185, psethu@uab.edu.

I. Introduction

Cardiac Tissue Chips (CTCs) can potentially be used as models of the heart to understand signaling mechanisms involved in cardiac development and disease and as models for cardiovascular drug development and testing. The heart constantly interacts with blood and any drug delivered systemically interacts with the myocardium. Given the importance of heart (pump) function, drug-induced cardiotoxicity (arrhythmia risk and compromised contractile function) has been a major reason for pharmaceutical withdrawal of FDA approved drugs [1]. Historically, the development of Cardiac Tissue Chip Models has been limited due to lack of *in vitro* cell culture systems that can reproduce hemodynamic loading and unloading associated with heart (pump) function. Hemodynamic loads are extremely important in embryonic heart development and in progression of cardiovascular disease and play a major role in both physiological hypertrophy (organ growth and maturation) as well as pathological hypertrophy (adverse remodeling and compromised myocardial function).

Cardiac cells have been cultured primarily using standard cell culture techniques in static conditions. While these techniques can provide biochemical stimuli, they fail to adequately replicate critical hemodynamic (mechanical) stresses experienced by cardiac cells *in vivo*. Commercially available systems include the FlexCell technology which imposes stretch stimulus on cultured cells, and IonOptix systems that provide the ability to either electrically stimulate or combine electrical stimulation with stretch. There have also been several groups that have developed technologies to mimic various aspects of the *in vivo* environment to enable differentiation and maturation of stem cell derived cardiomyocytes including mimicking geometric constraints [2], nanopatterning [3], culture in dense collagen matrices [4], culture in 3D fibrin gels [5], use of thyroid hormone and miRNAs [6, 7], use of passive or dynamic stretch and electrical stimulation [8], moderate afterload [9], ontomimetic differentiation [10] and electromechanical stimulation [11]. While these approaches have yielded varying levels of success from a standpoint of maturation and differentiation, these approaches still do not mimic the complex pressure-volume (PV) changes observed in the left-ventricle of the heart which is the location associated with most common cardiac pathologies. To address this issue we previously developed the cardiac cell culture model (CCCM) [12, 13] and the biomimetic cardiac tissue model (BCTM) [14] platforms which mimic PV loading associated with any chamber of the heart at any stage of development. However, we failed to mimic the predominantly uniaxial stretch mechanics and three dimensional (3D) and multicellular architecture associated with the ventricular wall. To develop the next generation of cardiac tissue culture systems, we developed the Cardiac Tissue Chip (CTC) which can not only reproduce uniaxial loading of and left ventricular PV loading associated with normal and pathological cardiac function but also accomplish culture of multi-cellular 3D tissue. Within the CTC, cardiomyocytes and fibroblasts are organized as 3D tissue within fibrin gels suspended between two posts. The engineered 3D tissue experiences cycles of stretch, contraction (pressure), ejection and relaxation similar to that observed during the cardiac cycle.

In cardiovascular disease, progression of pathological remodeling occurs in large part due to sustained non-physiological hemodynamic loads. The two most common manifestations of

non-physiological hemodynamic loads include pressure and volume overload. Pressure overload is associated with an increase in left-ventricular pressure that typically develops due to chronic hypertension as a consequence elevated systemic resistance and leads to hypertrophic cardiomyopathy (HCM) [15]. HCM manifests as uncontrolled hypertrophic growth of myocytes typically in an unorganized manner that leads to concentric cardiomyocyte hypertrophy (thickening) along with apoptosis [16–18]. Resulting cell death and hypertrophy coincide with increased fibrosis mediated by cardiac fibroblasts, oxidative stress and structural remodeling [19–21]. The increased matrix deposition disrupts normal cardiac conduction leading to increases in arrhythmia risks, and increased wall stiffness and thickness [22]. Cardiac fibroblasts play a central role in pathological hypertrophy seen in pressure overload by resisting the increases in wall stress through activation of TGF-β signaling and increased extracellular matrix (ECM) deposition [23]. Left ventricular volume overload occurs due to diastolic dysfunction or mitral regurgitation resulting in excess residual volume in the left ventricle causing thinning of the ventricular wall which leads to dilated cardiomyopathy (DCM) and ultimately heart failure [24]. Thinning of the ventricle leads to elongation of cardiomyocytes in the left ventricular wall that undergo eccentric hypertrophy.[25] The increase in stretch has been linked to matrix degradation, increase in reactive oxygen species (ROS), and disruption of cytoskeletal filament proteins involved in mechanotransduction. [26–29]

Given the importance of hemodynamic stresses as a consequence of PV changes within the left-ventricle, it is essential that disease models of cardiac tissue have the ability to accurately recreate pathological hemodynamic loads. While several systems and models exist to subject cultured cardiac cells to pressure or stretch [12, 13, 30, 31], none of these models mimic the complexity of loading associated with the cardiac cycle. The CTC therefore address the absence of relevant *in vitro* systems to recreate cardiac physiology and pathophysiology resulting from hemodynamic imbalances. By recreating the hemodynamics associated with the left-ventricle *in vivo* during both normal heart function and during cardiomyopathies (Fig. 1), it may be possible to develop new and relevant models of cardiovascular disease. Using these models, we can target the mechanotransduction pathways that result in pathological remodeling seen in hypertrophic and dilated cardiomyopathy for discovery and testing of new therapeutics. In this manuscript we detail the use of the CTC to create models of both pure pressure and pure volume overload and show that critical structural and functional changes associated with both these conditions can be reproduced. For model development we chose to use the h9c2 rat myoblast cell line which is widely used for cardiovascular disease modelling and can be maintained in culture for prolonged duration. The choice of h9c2 cells is relevant for modelling pressure overload as prior studies confirm that these cells are indeed responsive to hypertrophic signaling *in vitro* and appropriate to study the effects of pathological levels of pressure [32–34]. Despite the fact that these cells do not contract either spontaneously or under the influence of external pacing, these cells possess similar calcium channels, sarcomeric proteins, and metabolic profiles to cardiac cells [35–37]. H9c2 cells have also been used extensively to study myocardial infarctions and reperfusion injuries due to their similarities in comparison to *in vivo* responses to oxidative stress [38, 39]. In the context of this study, these cells provide an ideal cell type to accomplish development of cardiovascular disease models.

II. Materials and Methods

Cell Culture Chamber Fabrication

Cell culture chambers were fabricated using standard soft-lithography using (poly)dimethyl siloxane (PDMS) (Sylgard 184, Dow Corning, Midland, MI) using standard techniques in our laboratory [40]. Assembled chambers were autoclaved and filled with 2% molten agarose and allowed to cool and solidify. A dumbbell shape pattern was created via removal of agarose using a hole punch and scalpel. Finally, the chamber was seeded with fibrin encapsulated cells and allowed to cross-link. The agarose mold was removed following 24 hours in culture resulting in a cell laden fibrin gel suspended between two posts. Following hemodynamic stimulation the cell laden fibrin gel can be removed from the post and retains its form making further analysis simpler (Fig. 2A).

CTC Stimulation

The setup and working cycle of the CTC are the same as described in our prior work.[41] Briefly, dynamic pressure differences above and below the cell culture chamber membrane in conjunction with directional flow control valves were exploited to reproduce the cardiac cycle. This version is different from the prior model as it was adapted for culture of 3D tissue fibres suspended between two posts (Fig. 2B–C).

Cell Culture and Fibrin Gel Encapsulation

2.2×10^6 h9c2 and 1.0×10^6 primary rat cardiac fibroblasts (RFB) cells were mixed together into 300uL media containing a final concentration of 2mg/mL fibrinogen (Millipore 341576), 0.9 units thrombin (Millipore 605195) per mg fibrin (0.54 units/gel), and 2mM $CaCl_2$. The gels were allowed to polymerize for 30 minutes within the incubator before media was added. During the gel making process, and until completion of the experiment, the culture medium was supplemented with 5mg/mL aminocaproic acid (Acros 103301000) to inhibit fibrinolysis. Our choice of fibrin gels for construction of engineered cardiac tissue is based on prior work with fibrin gels which achieved a passive stiffness of ~ 26 kPa [42] which is comparable to passive stiffness of the adult human ventricle which is between 20–50 kPa [43, 44].

RNA qRT-PCR

After 48 hours of stimulation the cells are removed from the CTC and placed within 700μL Trizol and then flash frozen and maintained in liquid nitrogen until processing. Once all samples were collected, they were thawed at room temperature and immediately placed within a beadmill (BeadBug D1030) containing 1.0mm silica beads (Benchmark D1031–10) and milled for 30 seconds at speed 4000. RNA is then isolated using standard phenol-chloroform extraction methods, and cDNA is created using Maxima kit (K1671). Custom ThermoFisher Taq-Man array plates (4391528) were created under design ID RAAAADM and coupled with Applied Biosystems master mix (4369514). Plates were run on a QuantStudio 3.

Statistical Analysis

An unpaired t-test was used for the analysis of the gene expression and aspect ratio data with two-tailed significance set at $p \leq 0.05$.

III. Results

Pressure-Volume Changes Seen in Normal and Pathological Conditions

Using the CTC we were able to accurately replicate pressure-volume changes associated with normal, pure pressure overload and pure volume overload. Normal conditions were set to a 1Hz cardiac cycle with 100mmHg peak-systolic pressure, 10mmHg end-diastolic pressure, and a minimum strain of 0% and maximum strain of 2% (Fig. 3, left). Pressure overload conditions were set to a 1Hz cardiac cycle with 160mmHg peak-systolic pressure, 10mmHg end-diastolic pressure, and a minimum strain of 0% and a maximum strain of 2% (Fig. 3, middle). Volume overload conditions were set to a 1Hz cardiac cycle with 100mmHg peak-systolic pressure, 30mmHg end-diastolic pressure, and minimum strain of 2% and maximum strain of 7% (Fig. 3, right). To reproduce the hemodynamics of dilated cardiomyopathy the volume overload was not allowed to return to its resting level of strain in order to reproduce the constant wall stress seen *in vivo.*

Gross Tissue Morphology and Organization

At the conclusion of the experiment, fibers were evaluated for alignment and general tissue morphology using H&E staining of paraffin embedded slices of the fibers (Fig. 4). In all samples, regardless of the presence or absence of stimulation, the fiber contraction around the post caused alignment of the ECM resulting in cell alignment. H&E staining confirmed that cells were able to spread and evenly distribute throughout the tissue fiber. To determine if the experimental conditions were able to induce an increase in ECM deposition the slices of were also stained using Masson's trichrome stain (Fig. 5).

It is clear both from the 20X and 40X images that 48 hour stimulation within the BCTM under conditions of pressure overload results in a noticeable increase in collagen deposition along the center of the fiber.

Tissue Aspect Ratio after 7 Days of Stimulation

While changes in gene expression manifest within 48 hours, it was necessary to extend the duration of stimulation to 7 days to observe noticeable changes in tissue dimensions. Following 7 days of stimulation, the volume overload samples experienced a significant increase (18%) in total length of the fibre and this change can be seen in the kink in the fibre when returned to the original post position (Fig. 6). Measurement of the width of the fibres was used in conjunction with overall fibre length to estimate aspect ratios of the tissue fibres for each condition. The change in aspect ratios for the pressure overload and volume overload were significant when compared to the static control and normal sample (Fig. 6). These results show a striking similarity to *in vivo* observations where pressure overload induces an increase in aspect ratio (width/length) and volume overload induces thinning and elongation, thus decreasing the aspect ratio. For clarity, the longest dimension is considered the length in these measurements.

Gene Expression Profiling

Following the 48 hours of CTC stimulation, the changes in gene expression were profiled for static (N = 3), normal (N =3), pressure overload (N = 3) and volume overload (N =3). Our results show that there are indeed significant changes in the expression of various genes following culture under normal and pathological loading (Fig. 7). Genes were classified into four categories within the array. Profiling of genes associated with fibrosis found that Collagen I was significantly upregulated in the pressure overload samples whereas transforming growth factor beta (TGF-β) was significantly upregulated in both pressure overload and normally stimulated samples. Evaluation of genes associated with cytoskeletal filament proteins found that desmin was significantly upregulated in the volume overload samples. Finally, evaluation of genes associated with matrix remodelling and antioxidant signalling found that tissue inhibitors of matrix metalloproteases (TIMPs) 1 and 2 were upregulated under pressure overload conditions and a significant increase in superoxide dismutase (SOD) 1 and SOD2 in both pressure and volume overload samples. Data is represented as relative change with the expression of each gene normalized to GAPDH expression levels.

IV. Discussion

Cardiovascular disease modelling, drug testing and drug discovery have been significantly impacted by the absence of relevant in-vitro cell culture models to culture cardiac cells under physiological and pathophysiological pressure-volume loading. Cardiomyocytes and other cardiac cells rely on these mechanical stress signals to maintain homeostasis and ensure normal heart function. However, chronic exposure to pathological levels of either pressure or stress can result in activation of compensatory mechanisms that lead to maladaptive cardiac tissue remodeling. To accurately model cardiomyopathies associated with altered mechanical loading as in the cases of pure pressure or volume overload, it is essential to evaluate cardiac cells in an environment where pressure-volume changes seen in the dysfunctional myocardium can be accurately recreated. The CTC is a unique model system that accurately reproduces mechanical loads that drive progression of cardiac tissue remodeling and was used in this study to establish conditions of both pressure and volume overload to determine if maladaptive remodeling and molecular signaling mechanisms that drive structural and functional changes associated with either of these conditions can be accurately replicated in an in-vitro model system.

To enable mechanical stimulation of engineered 3D tissue, we developed a method for suspending 3D fibrin fibres composed of cardiac cells between a set of rigid polymeric posts mounted onto a thin polymeric membrane. Using this setup we achieved cellular alignment through the inherent compaction of the fibrin gel prior to imposition of any cyclic mechanical strain. This setup also allows for the application of uniaxial strain to the cells along their long axis during CTC stimulation. The natural alignment of the cells within the fibres ensured that the only difference between the stimulated and static samples was the imposition of hemodynamic loads.

Pressure overload is associated with concentric hypertrophy (thickening of myocytes), increased fibrosis, oxidative stress, and inflammation. After 7 days of stimulation under

conditions of pressure overload (160 mmHg, 2% strain) confirms that stimulated tissue undergoes hypertrophy, becoming thicker with an increased aspect ratio. Pressure overload also resulted in a significant increase in collagen deposition within the fibres as seen with Masson trichrome staining. This increase in collagen deposition was reinforced with gene expression studies confirming a statistically significant (~ 7 fold) increase in collagen i gene expression in comparison to static controls. Matrix metalloproteinases (MMPs) are responsible for the degradation of ECM proteins and tissue inhibitors of metalloproteinases (TIMPs) inhibit the ability of MMPs to degrade the ECM. Gene expression results show that both TIMP1 and TIMP2 were significantly upregulated in pressure overload samples whereas a statistically significant increase in MMPs was not observed suggesting that the change in the balance between TIMPs and MMPs favouring TIMPs indicates an environment favouring fibrosis in pressure overload. These results are similar to the pathophysiology of cardiac tissue remodelling *in vivo* where pressure overload induces a stiffening of the myocardial wall through collagen deposition and a thickening through myocyte hypertrophy. TGF-β is potent pro-fibrotic signalling molecule and is upregulated in both pressure and volume overload *in vivo* and results in increased ECM deposition and the differentiation of fibroblast into myofibroblasts [45–53]. In our studies we found that TGF-β was significantly upregulated only in the pressure overload and normal samples and not in the volume overload samples. The upregulation of TGF-β in the normal samples is most likely due to stress induced pathways; studies have shown that stretching cells can induce increases in TGF-β expression [54, 55].

Volume overload is associated with the thinning of the ventricular wall resulting in eccentric hypertrophy (myocyte thinning), significant matrix degradation, oxidative stress, and inflammation. Following 48 hours of stimulation under conditions of volume overload, we did not observe any significant difference in overall fibre length in comparison to the other conditions. The absence of a change in length of the volume overload sample after 48 hours led us to extend the duration of stimulation to 7 days. Following 7 days of stimulation under conditions of volume overload within the BCTM, the fibres were significantly longer (~ 18%) than the static, normal, and pressure samples. The increased stimulation time had no effect on the final lengths of the static, normal, and pressure samples. The resulting increase in length of the volume overload samples demonstrates the reproduction of the elongated tissue phenotype seen *in vivo* and suggests that progression of eccentric hypertrophy associated with ventricular wall thinning is a time dependent phenomenon. As expected, desmin was significantly upregulated in the volume overload samples. Desmin is an intermediate filament protein that functions as an important mechanosensor that connects the sarcomere through its Z-disk to the mitochondria, nucleus, ECM, through costameres and intercalated disks, and other organelles [56–58]. *In vivo* studies show that volume overload causes desmin to become damaged and disorganized resulting in increased transcriptional regulation [59, 60]. It is possible that volume overload induced damage to the cytoskeleton causes the activation of a compensatory mechanism to replace the damaged/broken down desmin [61, 62].

Both volume and pressure overload induced upregulation of SOD gene expression. SOD1 is typically localized in the cytoplasm whereas SOD2 in the located in the mitochondria. Hypertrophic and dilated cardiomyopathies have both been linked to an increase in

intracellular ROS *in vivo* [63–67]. Several studies have shown that an unchecked increase in intracellular ROS can lead to the tissue and cell damage seen in cardiomyopathies [68–70]. It is likely that the observed increase in in SOD at the transcript level is linked to a compensatory antioxidant response in cells subject to pressure and volume overload.

V. Conclusions

In conclusion, we provide evidence that the CTC can serve as a valuable model system via reproduction of the fundamental characteristics of hemodynamic stress associated with pure volume and pressure overload. These results clearly show that major structural and molecular changes associated with pressure and volume overload can be recreated and provide strong rationale for development of *in vitro* models of cardiac tissue where the pressure-volume associated with the cardiac cycle are used to study cardiovascular disease pathologies. While this study utilized H9c2 cells and primary cardiac fibroblasts, more relevant cells types including human induced pluripotent stem cell derived cardiomyocytes (hiPSC-CMs) and human embryonic stem cell derived cardiomyocytes (hESC-CMs) cultured within the CTC could be used to model human cardiovascular disease and cardiac tissue remodelling in response to changes in hemodynamics.

Acknowledgements

The authors would like to thank Dr. Min Xie for kindly providing primary cardiac fibroblasts, and Mr. Thomas A. Haglund and Ms. Ritika Samant for help with cell culture and microscopy. This work was supported by a National Institute of Health R21 grant # 11675980, funds from the University of Alabama at Birmingham Comprehensive Cardiovascular Center and Department of Biomedical Engineering. AJR was supported by NIH T32 training grant # 5T32HL007918-18.

References

[1]. Fermini B et al., “A New Perspective in the Field of Cardiac Safety Testing through the Comprehensive In Vitro Proarrhythmia Assay Paradigm,” J Biomol Screen, vol. 21, no. 1, pp. 1–11, 1, 2016. [PubMed: 26170255]

[2]. Pilarczyk G et al., “Tissue-Mimicking Geometrical Constraints Stimulate Tissue-Like Constitution and Activity of Mouse Neonatal and Human-Induced Pluripotent Stem Cell-Derived Cardiac Myocytes,” Journal of Functional Biomaterials, vol. 7, no. 1, pp. 1, 2016.

[3]. Carson D et al., “Nanotopography-Induced Structural Anisotropy and Sarcomere Development in Human Cardiomyocytes Derived from Induced Pluripotent Stem Cells,” ACS Applied Materials & Interfaces, 2016/2/11, 2016.

[4]. Roberts MA et al., “Stromal Cells in Dense Collagen Promote Cardiomyocyte and Microvascular Patterning in Engineered Human Heart Tissue,” Tissue Engineering Part A, vol. 22, no. 7–8, pp. 633–644, 2016/4/01, 2016. [PubMed: 26955856]

[5]. Zhang D et al., “Tissue-engineered cardiac patch for advanced functional maturation of human ESC-derived cardiomyocytes,” Biomaterials, vol. 34, no. 23, pp. 5813–20, 7, 2013. [PubMed: 23642535]

[6]. Parikh SS et al., “Thyroid and Glucocorticoid Hormones Promote Functional T-Tubule Development in Human-Induced Pluripotent Stem Cell-Derived Cardiomyocytes,” Circ Res, vol. 121, no. 12, pp. 1323–1330, 12 8, 2017. [PubMed: 28974554]

[7]. Kuppusamy KT et al., “Let-7 family of microRNA is required for maturation and adult-like metabolism in stem cell-derived cardiomyocytes,” Proceedings of the National Academy of Sciences, vol. 112, no. 21, pp. E2785–E2794, 2015.

[8]. Ruan JL et al., "Mechanical Stress Conditioning and Electrical Stimulation Promote Contractility and Force Maturation of Induced Pluripotent Stem Cell-Derived Human Cardiac Tissue," Circulation, vol. 134, no. 20, pp. 1557–1567, 11 15, 2016. [PubMed: 27737958]

[9]. Leonard A et al., "Afterload promotes maturation of human induced pluripotent stem cell derived cardiomyocytes in engineered heart tissues," Journal of Molecular and Cellular Cardiology, vol. 118, pp. 147–158, 2018/5/01/, 2018. [PubMed: 29604261]

[10]. Kerscher P et al., "Direct hydrogel encapsulation of pluripotent stem cells enables ontomimetic differentiation and growth of engineered human heart tissues," Biomaterials, vol. 83, pp. 383–395, 3//, 2016. [PubMed: 26826618]

[11]. Ronaldson-Bouchard K et al., "Advanced maturation of human cardiac tissue grown from pluripotent stem cells," Nature, vol. 556, no. 7700, pp. 239–243, 4, 2018. [PubMed: 29618819]

[12]. Nguyen MD et al., "Effects of physiologic mechanical stimulation on embryonic chick cardiomyocytes using a microfluidic cardiac cell culture model," Anal Chem, vol. 87, no. 4, pp. 2107–13, 2 17, 2015. [PubMed: 25539164]

[13]. Nguyen MD et al., "Cardiac cell culture model as a left ventricle mimic for cardiac tissue generation," Anal Chem, vol. 85, no. 18, pp. 8773–9, 9 17, 2013. [PubMed: 23952579]

[14]. Rogers AJ et al., "Biomimetic Cardiac Tissue Model Enables the Adaption of Human Induced Pluripotent Stem Cell Cardiomyocytes to Physiological Hemodynamic Loads," Anal Chem, vol. 88, no. 19, pp. 9862–9868, 10 4, 2016. [PubMed: 27620367]

[15]. Matsushita N et al., "Chronic Pressure Overload Induces Cardiac Hypertrophy and Fibrosis via Increases in SGLT1 and IL-18 Gene Expression in Mice," Int Heart J, 8 11, 2018.

[16]. Anversa P et al., "Cellular basis of ventricular remodeling in hypertensive cardiomyopathy," Am J Hypertens, vol. 5, no. 10, pp. 758–70, 10, 1992. [PubMed: 1418841]

[17]. Schwartzkopff B et al., "Heart failure on the basis of hypertension," Circulation, vol. 87, no. 5 Suppl, pp. Iv66–72, 5, 1993. [PubMed: 8485835]

[18]. Swynghedauw B, "Remodeling of the heart in chronic pressure overload," Basic Res Cardiol, vol. 86 Suppl 1, pp. 99–105, 1991.

[19]. Creemers EE, and Pinto YM, "Molecular mechanisms that control interstitial fibrosis in the pressure-overloaded heart," Cardiovasc Res, vol. 89, no. 2, pp. 265–72, 2 1, 2011. [PubMed: 20880837]

[20]. Maulik SK, and Kumar S, "Oxidative stress and cardiac hypertrophy: a review," Toxicol Mech Methods, vol. 22, no. 5, pp. 359–66, 6, 2012. [PubMed: 22394344]

[21]. Weber KT et al., "Patterns of myocardial fibrosis," J Mol Cell Cardiol, vol. 21 Suppl 5, pp. 121–31, 12, 1989. [PubMed: 2534137]

[22]. Khan R, and Sheppard R, "Fibrosis in heart disease: understanding the role of transforming growth factor-beta in cardiomyopathy, valvular disease and arrhythmia," Immunology, vol. 118, no. 1, pp. 10–24, 5, 2006. [PubMed: 16630019]

[23]. Fujiu K, and Nagai R, "Fibroblast-mediated pathways in cardiac hypertrophy," Journal of Molecular and Cellular Cardiology, vol. 70, pp. 64–73, 2014/5/01/, 2014. [PubMed: 24492068]

[24]. Mohamed BA et al., "Molecular and structural transition mechanisms in long-term volume overload," Eur J Heart Fail, vol. 18, no. 4, pp. 362–71, 4, 2016. [PubMed: 26694078]

[25]. Liu Y et al., "Volume overload induces differential spatiotemporal regulation of myocardial soluble guanylyl cyclase in eccentric hypertrophy and heart failure," J Mol Cell Cardiol, vol. 60, pp. 72–83, 7, 2013. [PubMed: 23567617]

[26]. Barnes J, and Dell'Italia LJ, "The multiple mechanistic faces of a pure volume overload: implications for therapy," Am J Med Sci, vol. 348, no. 4, pp. 337–46, 10, 2014. [PubMed: 24781435]

[27]. Reddy S, and Bernstein D, "Molecular Mechanisms of Right Ventricular Failure," Circulation, vol. 132, no. 18, pp. 1734–42, 11 3, 2015. [PubMed: 26527692]

[28]. Barnes J et al., "Whole-genome profiling highlights the molecular complexity underlying eccentric cardiac hypertrophy," Ther Adv Cardiovasc Dis, vol. 8, no. 3, pp. 97–118, 3 31, 2014. [PubMed: 24692245]

[29]. Gladden JD et al., "Oxidative stress and myocardial remodeling in chronic mitral regurgitation," Am J Med Sci, vol. 342, no. 2, pp. 114–9, 8, 2011. [PubMed: 21795957]

[30]. De Jong AM et al., “Cyclical stretch induces structural changes in atrial myocytes,” J Cell Mol Med, vol. 17, no. 6, pp. 743–53, 6, 2013. [PubMed: 23617620]

[31]. Ferroni M et al., “Modeling the fluid-dynamics and oxygen consumption in a porous scaffold stimulated by cyclic squeeze pressure,” Med Eng Phys, vol. 38, no. 8, pp. 725–32, 8, 2016. [PubMed: 27189671]

[32]. Watkins SJ et al., “The H9C2 cell line and primary neonatal cardiomyocyte cells show similar hypertrophic responses in vitro,” In Vitro Cellular & Developmental Biology-Animal, vol. 47, no. 2, pp. 125–131, 2011. [PubMed: 21082279]

[33]. Vindis C et al., “Essential role of TRPC1 channels in cardiomyoblasts hypertrophy mediated by 5-HT 2A serotonin receptors,” Biochemical and biophysical research communications, vol. 391, no. 1, pp. 979–983, 2010. [PubMed: 20005206]

[34]. Xie F et al., “A static pressure sensitive receptor APJ promote H9c2 cardiomyocyte hypertrophy via PI3K-autophagy pathway,” Acta Biochim Biophys Sin, vol. 46, no. 8, pp. 699–708, 2014. [PubMed: 24966188]

[35]. Hescheler J et al., “Morphological, biochemical, and electrophysiological characterization of a clonal cell (H9c2) line from rat heart,” Circulation research, vol. 69, no. 6, pp. 1476–1486, 1991. [PubMed: 1683272]

[36]. Sipido KR, and Marban E, “L-type calcium channels, potassium channels, and novel nonspecific cation channels in a clonal muscle cell line derived from embryonic rat ventricle,” Circulation research, vol. 69, no. 6, pp. 1487–1499, 1991. [PubMed: 1659501]

[37]. Branco AF et al., “Gene expression profiling of H9c2 myoblast differentiation towards a cardiac-like phenotype,” PloS one, vol. 10, no. 6, pp. e0129303, 2015. [PubMed: 26121149]

[38]. Shan Z-X et al., “Upregulated expression of miR-1/miR-206 in a rat model of myocardial infarction,” Biochemical and biophysical research communications, vol. 381, no. 4, pp. 597–601, 2009. [PubMed: 19245789]

[39]. Wu X et al., “Impaired autophagy contributes to adverse cardiac remodeling in acute myocardial infarction,” PLoS One, vol. 9, no. 11, pp. e112891, 2014. [PubMed: 25409294]

[40]. Parichehreh V et al., “Microfluidic inertia enhanced phase partitioning for enriching nucleated cell populations in blood,” Lab Chip, vol. 13, no. 5, pp. 892–900, 3 7, 2013. [PubMed: 23307172]

[41]. Rogers AJ et al., “Biomimetic Cardiac Tissue Model Enables the Adaption of Human Induced Pluripotent Stem Cell Cardiomyocytes to Physiological Hemodynamic Loads,” Analytical Chemistry, vol. 88, no. 19, pp. 9862–9868, 2016. [PubMed: 27620367]

[42]. Shadrin IY et al., “Cardiopatch platform enables maturation and scale-up of human pluripotent stem cell-derived engineered heart tissues,” Nature communications, vol. 8, no. 1, pp. 1825–1825, 2017.

[43]. Fan L et al., “Infarcted Left Ventricles Have Stiffer Material Properties and Lower Stiffness Variation: Three-Dimensional Echo-Based Modeling to Quantify In Vivo Ventricle Material Properties,” J Biomech Eng, vol. 137, no. 8, pp. 081005, 8, 2015. [PubMed: 25994130]

[44]. Neagoe C et al., “Gigantic variety: expression patterns of titin isoforms in striated muscles and consequences for myofibrillar passive stiffness,” J Muscle Res Cell Motil, vol. 24, no. 2–3, pp. 175–89, 2003. [PubMed: 14609029]

[45]. Dobaczewski M et al., “Transforming growth factor (TGF)-beta signaling in cardiac remodeling,” J Mol Cell Cardiol, vol. 51, no. 4, pp. 600–6, 10, 2011. [PubMed: 21059352]

[46]. Li J-M, and Brooks G, “Differential Protein Expression and Subcellular Distribution of TGFβ1, β2 and β3 in Cardiomyocytes During Pressure Overload-induced Hypertrophy,” Journal of Molecular and Cellular Cardiology, vol. 29, no. 8, pp. 2213–2224, 1997/8/01/, 1997. [PubMed: 9281452]

[47]. Rosenkranz S et al., “Alterations of β-adrenergic signaling and cardiac hypertrophy in transgenic mice overexpressing TGF-β1,” American Journal of Physiology-Heart and Circulatory Physiology, vol. 283, no. 3, pp. H1253–H1262, 2002. [PubMed: 12181157]

[48]. Brooks A et al., “Interstitial fibrosis in the dilated non-ischaemic myocardium,” Heart, vol. 89, no. 10, pp. 1255–6, 10, 2003. [PubMed: 12975439]

[49]. Desmoulière A et al., “Transforming growth factor-beta 1 induces alpha-smooth muscle actin expression in granulation tissue myofibroblasts and in quiescent and growing cultured fibroblasts,” The Journal of Cell Biology, vol. 122, no. 1, pp. 103–111, 1993. [PubMed: 8314838]

[50]. et al DRP., “Differential expression of cytokines in the rat heart in response to sustained volume overload,” European Journal of Heart Failure, vol. 6, no. 6, pp. 693–703, 2004. [PubMed: 15542404]

[51]. Villarreal FJ, and Dillmann WH, “Cardiac hypertrophy-induced changes in mRNA levels for TGF-beta 1, fibronectin, and collagen,” American Journal of Physiology-Heart and Circulatory Physiology, vol. 262, no. 6, pp. H1861–H1866, 1992.

[52]. Calderone A et al., “Pressure-and volume-induced left ventricular hypertrophies are associated with distinct myocyte phenotypes and differential induction of peptide growth factor mRNAs,” Circulation, vol. 92, no. 9, pp. 2385–2390, 1995. [PubMed: 7586335]

[53]. Pauschinger M et al., “Dilated cardiomyopathy is associated with significant changes in collagen type I/III ratio,” Circulation, vol. 99, no. 21, pp. 2750–6, 6 1, 1999. [PubMed: 10351968]

[54]. Riser BL et al., “Cyclic stretching force selectively up-regulates transforming growth factor-beta isoforms in cultured rat mesangial cells,” The American Journal of Pathology, vol. 148, no. 6, pp. 1915–1923, 1996. [PubMed: 8669477]

[55]. van Wamel AJET et al., “Stretch-induced paracrine hypertrophic stimuli increase TGF-β1 expression in cardiomyocytes,” Molecular and Cellular Biochemistry, vol. 236, no. 1, pp. 147–153, 7 01, 2002. [PubMed: 12190114]

[56]. Milner DJ et al., “The absence of desmin leads to cardiomyocyte hypertrophy and cardiac dilation with compromised systolic function,” Journal of molecular and cellular cardiology, vol. 31, no. 11, pp. 2063–2076, 1999. [PubMed: 10591032]

[57]. Capetanaki Y et al., “Desmin Related Disease: A Matter of Cell Survival Failure,” Current opinion in cell biology, vol. 0, pp. 113–120, 02/11, 2015.

[58]. Charrier Elisabeth E. et al., “Desmin Mutation in the C-Terminal Domain Impairs Traction Force Generation in Myoblasts,” Biophysical Journal, vol. 110, no. 2, pp. 470–480, 01/19 06/12/ received 11/23/accepted, 2016. [PubMed: 26789769]

[59]. Heling A et al., “Increased expression of cytoskeletal, linkage, and extracellular proteins in failing human myocardium,” Circ Res, vol. 86, no. 8, pp. 846–53, 4 28, 2000. [PubMed: 10785506]

[60]. Guichard JL et al., “Desmin loss and mitochondrial damage precede left ventricular systolic failure in volume overload heart failure,” Am J Physiol Heart Circ Physiol, vol. 313, no. 1, pp. H32–h45, 7 1, 2017. [PubMed: 28455287]

[61]. Weisleder N et al., “Cardiomyocyte-specific desmin rescue of desmin null cardiomyopathy excludes vascular involvement,” Journal of Molecular and Cellular Cardiology, vol. 36, no. 1, pp. 121–128, 2004/1/01/, 2004. [PubMed: 14734054]

[62]. Wang X et al., “Mouse Model of Desmin-Related Cardiomyopathy,” Circulation, vol. 103, no. 19, pp. 2402–2407, 2001. [PubMed: 11352891]

[63]. Takimoto E, and Kass DA, “Role of oxidative stress in cardiac hypertrophy and remodeling,” Hypertension, vol. 49, no. 2, pp. 241–248, 2007. [PubMed: 17190878]

[64]. Dhalla AK et al., “Role of oxidative stress in transition of hypertrophy to heart failure,” Journal of the American College of Cardiology, vol. 28, no. 2, pp. 506–514, 1996. [PubMed: 8800132]

[65]. Seddon M et al., “Oxidative stress and redox signalling in cardiac hypertrophy and heart failure,” Heart, vol. 93, no. 8, pp. 903–907, 2007. [PubMed: 16670100]

[66]. Giordano FJ, “Oxygen, oxidative stress, hypoxia, and heart failure,” The Journal of clinical investigation, vol. 115, no. 3, pp. 500–508, 2005. [PubMed: 15765131]

[67]. Münzel T et al., “Pathophysiological role of oxidative stress in systolic and diastolic heart failure and its therapeutic implications,” European heart journal, vol. 36, no. 38, pp. 2555–2564, 2015. [PubMed: 26142467]

[68]. Liu Z-W et al., “Protein kinase RNA-like endoplasmic reticulum kinase (PERK) signaling pathway plays a major role in reactive oxygen species (ROS)-mediated endoplasmic reticulum

stress-induced apoptosis in diabetic cardiomyopathy," Cardiovascular diabetology, vol. 12, no. 1, pp. 158, 2013. [PubMed: 24180212]

[69]. Ungvari Z et al., "Role of oxidative-nitrosative stress and downstream pathways in various forms of cardiomyopathy and heart failure," Current vascular pharmacology, vol. 3, no. 3, pp. 221–229, 2005. [PubMed: 16026319]

[70]. Liu M et al., "Mitochondrial dysfunction causing cardiac sodium channel downregulation in cardiomyopathy," Journal of molecular and cellular cardiology, vol. 54, pp. 25–34, 2013. [PubMed: 23123323]

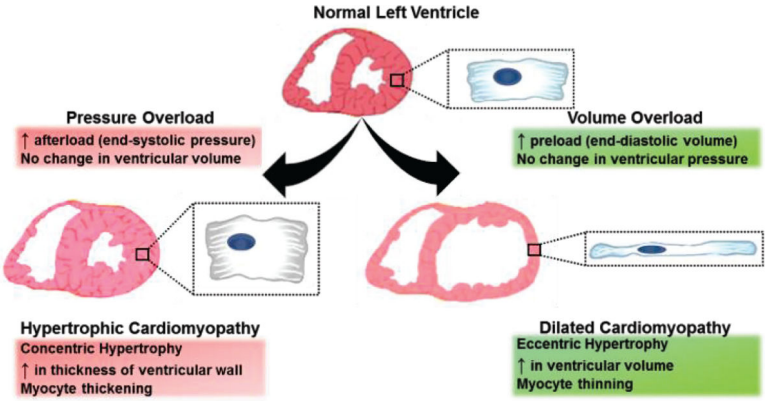

Figure 1. Pressure and Volume Overload.

Pressure overload is associated with an increase in end systolic pressure that causes an increase in the ventricular wall thickness through myocyte thickening caused by sarcomere addition. Volume overload occurs when the end diastolic volume is increased leading to a constant increase in residual ventricular volume that over time causes wall thinning through myocyte thinning and elongation.

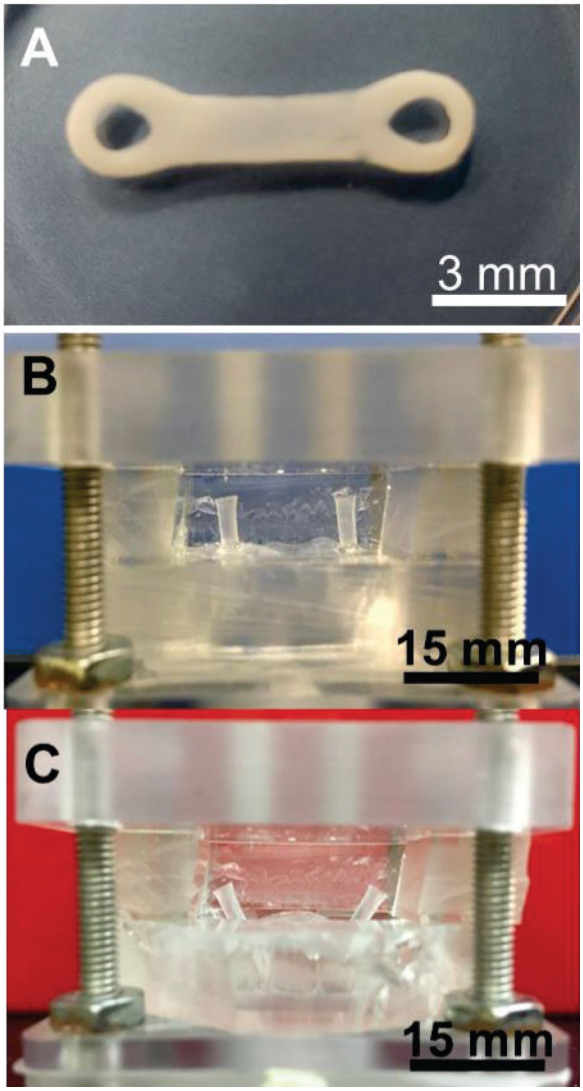

Figure 2. Images of the Cell Culture Chamber.

(A) This image was taken 2 days after removing the agarose mold and removing the cell laden fibrin gel from the two posts. The gel originally forms around the posts and takes the shape of the agarose mold but contracts over time. Once the gel contracts away from the agarose mold it becomes a free standing fiber suspended between two posts **(B)** The position of the posts within the cell culture chamber at the end of systole. The fiber experiences no strain at this point as the posts are at the initial resting position. **(C)** Position of posts within the cell culture chamber at the end of diastole. The thin membrane contacts with the insert below and deforms along its surface thus pulling the posts away from each other and applying uniaxial strain to the fiber. **(Scale = 4 mm)**

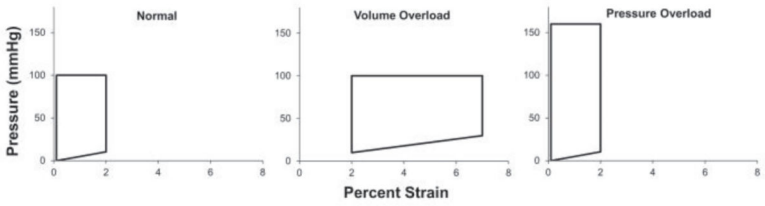

Figure 3. H9c2 Pressure-Volume loops.

Plots of the pressure vs. percentage strain that H9c2 cells were subjected to within the CTC during the course of an experiment. The pressure and percentage strain were gradually increased over the course of 1 hour until the final pressure and strain values shown in the plots were obtained and maintained at that level until the conclusion of the experiment.

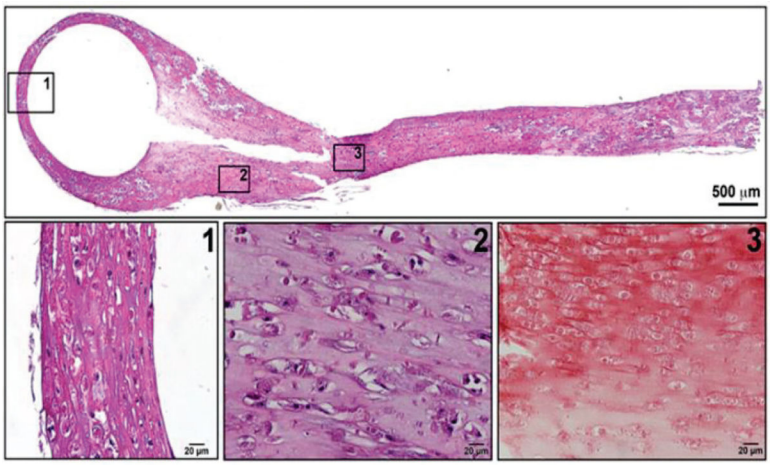

Figure 4. Gross Morphology and Alignment.

H&E staining of paraffin embedded tissue sections show alignment and uniform distribution of H9c2 cells within the fibre regardless of location of the fibre. The image shown is from a sample subjected to normal pressure-volume loading but the alignment and organization are representative of all samples including static, pressure overload, and volume overload samples. **(Scale: Top = 500 μm, Bottom = 50 μm)**

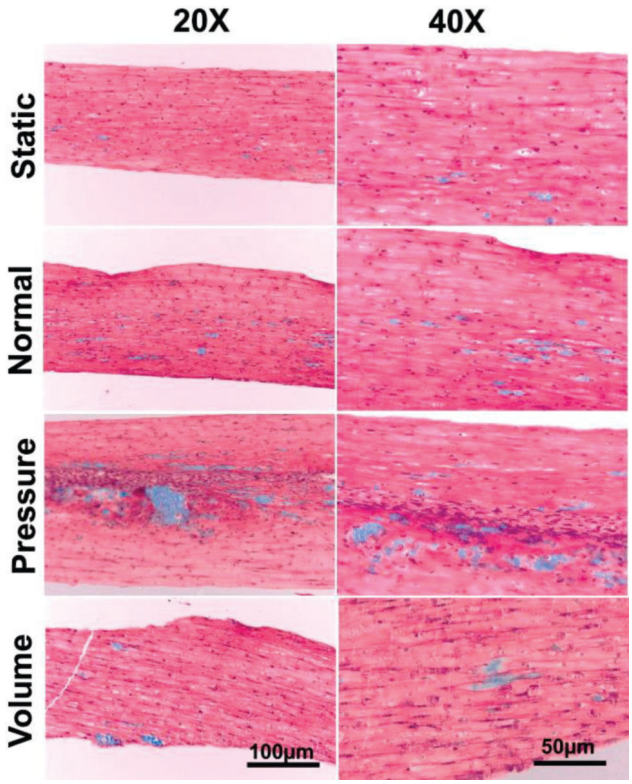

Figure 5. Masson's Trichrome Staining.

Paraffin embedded and sectioned H9c2 fibres were imaged following Masson's trichrome staining. **(Static)** Unstimulated tissue fibre that was maintained in static culture. **(Normal, Pressure, and, Volume)** Tissue fibres stimulated within the CTC under normal, pressure overload, and volume overload conditions respectively. The pressure overload sample shows significant increases in fibrosis along the center line of the fibre and is clearly thicker than the other samples. Thinning is also noted in the volume overload sample. There were minimal levels of fibrosis within the static, normal, and volume overload fibres. **(Scale: Left = 100 μm, Right = 50 μm)**

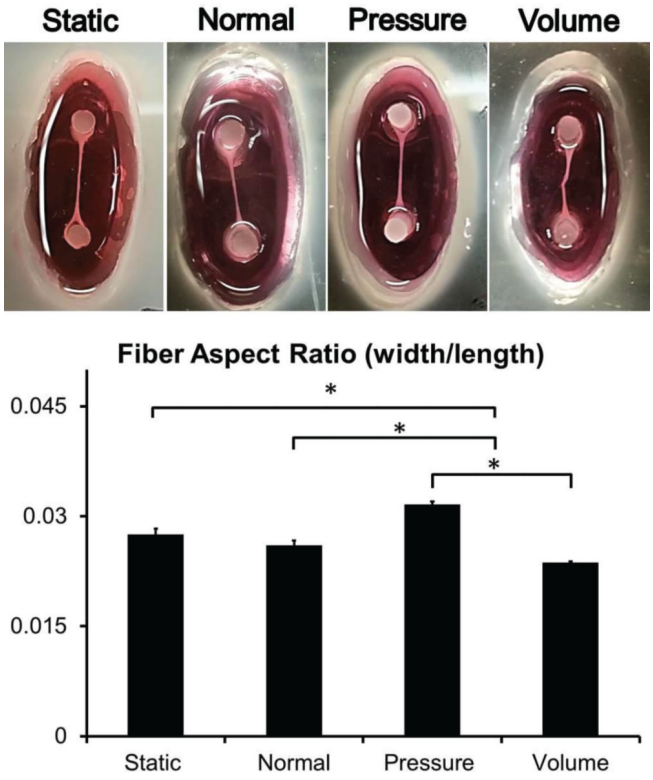

Figure 6. Aspect Ratio Measurements.

Static, normal, volume overload, and pressure overload samples labelled ‘static’, ‘normal’, ‘pressure’, and ‘volume’ respectively (N=5 for each group). The volume overload showed a significant increase in length and is clearly elongated in the image so much so that it has buckled once it returned to its original resting state. The increase in length resulted in a significant decrease in aspect ratio compared to static, normal, and pressure overload samples. Pressure overload samples significantly increased in width but not length, resulting in a significant increase in aspect ratio when compared to static, normal, and volume overload samples. The difference between normal and static samples was not significant although a decrease in aspect ratio was found in the normal samples. **(Scale = 4 mm)**

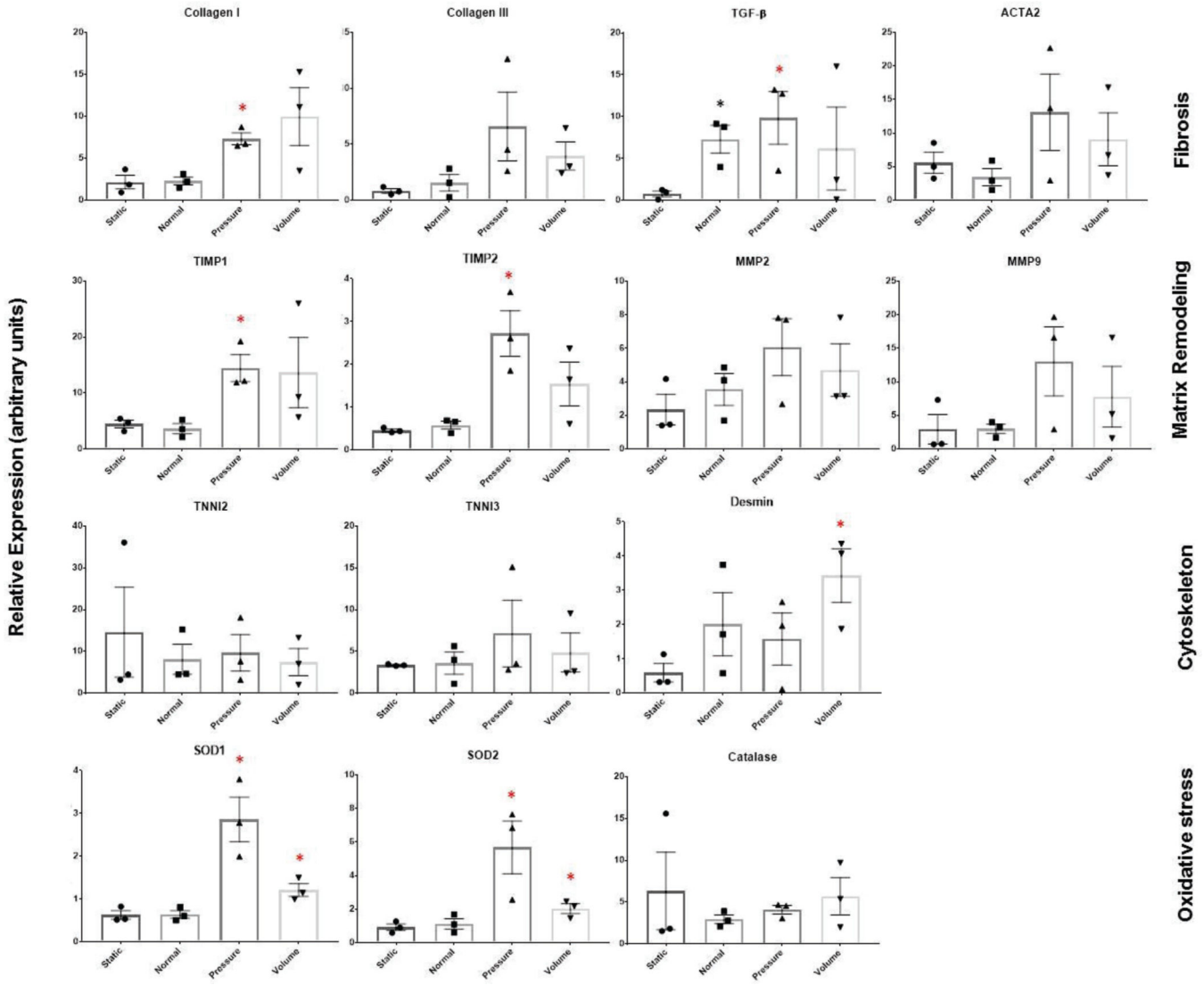

Figure 7. Gene Expression Profiling.

Results from qRT-PCR array on H9c2 cells stimulated for 48 hours under static (N=3), normal (N=3), volume overload (N=3), and pressure overload (N=3) hemodynamics. Genes are classified into 4 categories, 'Fibrosis', 'Extracellular matrix remodelling', Cytoskeleton', and 'Antioxidants'. All genes were normalized to GAPDH levels.